MONTE CARLO SIMULATION AND ANALYSIS OF ROUND-TRIP TURBULENCE EFFECTS ON LADAR FOR UNRESOLVED TARGET DETECTION

March 1997

Douglas G. Youmans
W. J. Schafer Assoc.
321 Billerica Rd., Chelmsford, MA 01824

V. S. Rao Gudimetla
Oregon Graduate Institute
20000 NW Walker Rd., Portland OR 97291

ABSTRACT

The effects of round-trip atmospheric turbulence on ladar are being investigated using a Monte Carlo code with many phase-screens to simulate atmospheric turbulence effects. These phase-screens are located along the outward path of the laser-mode and the inward path of the backscattered laser speckle pattern. The targets used are variable in size and smaller than the propagated laser-mode transverse dimension and are therefore termed "unresolved." In this paper previous round-trip turbulence analyses and data are reviewed, and the current Monte Carlo simulation code is discussed. Simulation results to date are presented indicating that intensity fluctuations or "scintillation" is best described by a new two-parameter K-distribution probability density function. This intensity distribution may then be used in deriving a ladar receiver-operating-characteristic for determining the target detection probability including round-trip turbulence.

1.0 INTRODUCTION

Ladars operating within the atmosphere must transmit a laser mode through the atmosphere to the target. This mode is corrupted by turbulence which results in the familiar "atmospheric speckle" patterns on the target. Almost all atmospheric turbulence research to date has pertained to this one-way propagation problem. However, small diffuse or specular targets backscatter only a small fraction of the speckle pattern at long ranges when the target is angularly unresolved. This backscattered light then propagates back through the atmospheric turbulence, undergoing further corruption and is collected by the receiving aperture. Round-trip passage through turbulence causes a scintillation peak and then eventually saturating at a lower level as a funcion of target range. Aperture averaging of this round-trip speckle also occurs.

Measurements and analyses of round-trip turbulence intensity fluctuations for fully **resolved** targets were made in the 1980's by Gudimetla and Holmes[1-4] of the Oregon Graduate Institute. A "poly-chromatic K distribution" and a "mono-chromatic K distribution" were found to agree with data and theory for direct and heterodyne detection ladar irradiance fluctuations, respectively. These distributions were not incorporated into a ladar receiver-operating-characteristic analysis, however. Other measurements to very small glint (**un**resolved) targets were made at this time[5,6] which indicated enhanced intensity fluctuations-- a factor of 3 or 4 times larger normalized intensity variance.

Report Documentation Page

Report Date	Report Type	Dates Covered (from... to)
01MAR1997	N/A	-

Title and Subtitle Monte Carlo Simulation and Analysis of Round-Trip Turbulence Effects on Ladar for Unresolved Target Detection	**Contract Number**
	Grant Number
	Program Element Number
Author(s) Youmans, Douglas G.; Gudimetla, V. S. Rao	**Project Number**
	Task Number
	Work Unit Number
Performing Organization Name(s) and Address(es) W. J. Schafer Assoc. 321 Billerica Rd. Chelmsford, MA 01824	**Performing Organization Report Number**
Sponsoring/Monitoring Agency Name(s) and Address(es) Director, CECOM RDEC Night Vision and Electronic Sensors Directorate, Security Team 10221 Burbeck Road Ft. Belvoir, VA 22060-5806	**Sponsor/Monitor's Acronym(s)**
	Sponsor/Monitor's Report Number(s)
Distribution/Availability Statement Approved for public release, distribution unlimited	
Supplementary Notes See Also ADM201040 (1997 IRIS Proceedings on CD-ROM).	
Abstract	
Subject Terms	
Report Classification unclassified	**Classification of this page** unclassified
Classification of Abstract unclassified	**Limitation of Abstract** SAR
Number of Pages 14	

The round-trip turbulence to small targets problem is now being studied using Monte Carlo techniques. Multiple large dimension phase-screens are used in propagating the laser mode to the target to simulate atmospheric turbulence. The phase-screens incorporate C_n^2, inner-scale dimension, outer-scale dimension, and laser wavelength in a modified Kolmogorov spectrum to accurately simulate path integrated turbulence effects. At the target, a subset of points diffusely or specularly reflects the laser speckle pattern. The backscattered E-field is then back-propagated through the same or new phase-screens and collected by a subset of points corresponding to the collection aperture. The irradiance fluctuations across this selectable aperture result in irradiance probability density functions, following many Monte Carlo runs. The simulated PDF's are compared to lognormal, negative-exponential, K-distribution, and other PDF models as a function of aperture size, path integrated turbulence strength, and target size. The correct irradiance PDF can then be incorporated into a ladar receiver-operating-characteristic. The smoothing effects of transverse wind is also demonstrated.

2.0 REVIEW OF THE ANALYTICAL TREATMENT OF ROUND-TRIP TURBULENCE

The analytical treatment of laser light propagation through round-trip turbulence is complicated. We review this treatment for purposes of summarizing the previous work for convenient reference and for comparing it to the results of the Monte Carlo code outputs.

2.1 Treatment of the E-field Propagation Through Turbulence (Round-Trip)

The laser radar transmitted E-field propagates out to the target where it is diffusely reflected (for the most common type of target) or specularly reflected by a glint or corner cube in some instances. The E-fields are propagated using an atmospheric Green's function integral formulation. The Green's function for the vacuum wave equation is

$$G(\vec{\rho}_2;\vec{\rho}_1,k) = \frac{1}{4\pi|\vec{\rho}_2-\vec{\rho}_1|}\exp(ik|\vec{\rho}_2-\vec{\rho}_1|) \qquad \textbf{(1)}$$

where $\vec{\rho}_1$ and $\vec{\rho}_2$ are vectors to the initial and final propagation points with wave number $k = 2\pi/\lambda$. Using the extended Huygens-Fresnel approximation and including atmospheric turbulence perturbations, the atmospheric Green's function is usually modeled by

$$G(\vec{\rho}_2;\vec{\rho}_1,L) \approx \frac{-i}{\lambda L}\exp(ikL)\exp\left(ik(\vec{\rho}_2-\vec{\rho}_1)^2/2L\right)\exp\left(\chi(\vec{\rho}_2,\vec{\rho}_1)+i\phi(\vec{\rho}_2,\vec{\rho}_1)\right) \qquad \textbf{(2)}$$

where

$\chi(\vec{r}_2,\vec{r}_1)$ and $\phi(\vec{r}_2,\vec{r}_1)$ are the log-amplitude and phase perturbations,

and $\vec{r}_1$, and $\vec{r}_2$ are radial vectors perpendicular to the propagation axis at 0 and L meters, respectively. The propagated E-field at a distance L is then given by the integral over the Green's function:

$$E(\vec{\rho}_2) = \int d\vec{\rho}_1\, G(\vec{\rho}_2;\vec{\rho}_1,L)\,E(\vec{\rho}_1) \qquad \textbf{(3)}$$

If we assume the transmitted laser beam is an unobscured, unclipped Gaussian, then the source E-field is

$$E_o(\vec{\rho}_1) = E_o\exp(-r_1^2/\omega^2 - ik\,r_1^2/2F) \qquad \textbf{(4)}$$

where ω is the $1/e^2$ intensity radius, F is the effective focal length, and $\vec{r}_1$ is the transverse coordinate at the transmitter aperture. The field at the target before reflection from the target is from equation (3)

$$E'(\vec{\rho}_2) = \frac{-ik}{2\pi L}\exp(ik(L+r_2^2/2L))\int E_o(\vec{\rho}_1)\exp(ik(r_1^2-2\vec{\rho}_1\bullet\vec{\rho}_2)/2L+\psi(\vec{\rho}_2,\vec{\rho}_1))d\vec{\rho}_1 \qquad \textbf{(5)}$$

where ψ is the sum of χ and $i\phi$. After reflection, the field is denoted by $E(\vec{r}_2)$. The E-field back at the receiver is then

$$E(\vec{\rho}_3) = \frac{-ik}{2\pi L} \exp(ik(L + r_3^2/2L)) \int E(\vec{\rho}_2) \exp\left(ik(r_2^2 - 2\vec{\rho}_2 \bullet \vec{\rho}_3)/2L + \psi(\vec{\rho}_3, \vec{\rho}_2)\right) d\vec{\rho}_2 \quad \textbf{(6)}$$

Holmes et al[1-3] have derived the time-delayed correlation function for the round-trip intensity

$$B_I(\vec{\rho}_3, \vec{\rho}_{3'}, \tau) = \left\langle E(\vec{\rho}_3, 0)\ E^*(\vec{\rho}_3, 0)\, E(\vec{\rho}_{3'}, \tau)\ E^*(\vec{\rho}_{3'}, \tau) \right\rangle \quad \textbf{(7)}$$

since many of the desired statistics can be determined from this function. Substituting $E(\vec{r}_2)$ into equation (6) and taking advantage of the diffuse target reflectivity properties

$$< E(\vec{\rho}_2) E^*(\vec{\rho}_{2'}) > = \frac{\lambda^2}{\pi} \rho_d < I(\vec{\rho}_2) > \delta(\vec{\rho}_2 - \vec{\rho}_{2'}) \quad \textbf{(8)}$$

as well as the jointly Gaussian nature of the reflected fields, Holmes calculates the time-delayed (round-trip) intensity covariance from equation (7),

$$C_I(\delta\vec{\rho}_3, \tau) = B_I(\delta\vec{\rho}_3, \tau) - < I >^2, \quad \textbf{(9)}$$

where $\delta\vec{r}_3 = \vec{r}_3 - \vec{r}_3'$, which he then averages over the receiving aperture. The aperture-averaged intensity variance with $\delta\vec{r}_3 = 0$ and $\tau = 0$ is reviewed in the next three sections.

2.2 Aperture Averaging of Atmospheric Scintillations

The large aperture of the receiving telescope averages the intensity fluctuations produced by atmospheric scintillation. The aperture averaged log-amplitude variance has been experimentally found to saturate at a value of about 0.5, which is, therefore, the maximum allowable value regardless of how large the Rytov point log-amplitude variance may be. The normalized intensity variance or "scintillation index" is defined as

$$\sigma_{I_n^2} \equiv \left(< I^2 > - < I >^2 \right) / < I >^2 \quad \textbf{(10)}$$

and is found from equation (9) with $C_I(\delta r_3 = 0, \tau = 0)$, shown by Holmes to be

$$\sigma_{I_n}^2 = \left(\frac{k}{L}\right)^2 \int_o^\infty \int_o^\infty r dr d\, r_2 d\theta\, r_2 \left(2 \exp[4 C_c(\vec{\rho}_3, \vec{\rho}_2, 0)] - 1\right) J_0\left(\frac{k}{L} \theta\, r_2 r\right) f_2(r) \quad \textbf{(11)}$$

where $f_2(r)$ is defined

$$f_2(r) = \exp\left(-r^2 \left(\frac{1}{2\omega^2} + \left[\frac{k\omega}{2L} \left(1 - \frac{L}{F} \right) \right]^2 \right) - 2 \left(\frac{r}{1.5\rho_o} \right)^{5/3} \right) \quad \textbf{(12)}$$

where ω is the $1/e^2$ intensity radius of the transmitter beam ($\omega \approx d_{tran}/2$), F is the effective focal length (phase-front curvature), and we use the definition of ρ_o

$$r_o = \left[2.91 k^2 \int_o^R dz\ C_n^2(z) (1 - z/R)^{5/3} \right]^{-3/5} \quad \textbf{(13)}$$

which for constant C_n^2 this becomes

$$\rho_o = \left[1.09 k^2 C_n^2 R \right]^{-3/5} \quad (C_n^2 \text{ constant}) \quad \textbf{(14)}$$

$C_\chi(\delta\vec{r}_3, \delta\vec{r}_2, \vec{v}\tau)$ is the log-amplitude covariance function defined as

$$C_c(\vec{\rho}_3, \vec{\rho}_2, \vec{v}t) \equiv \left\langle \left(c(0,0,0) - \left\langle c(0,0,0) \right\rangle \right) \left(c(\vec{\rho}_3, \vec{\rho}_2, \vec{v}t) - \left\langle c(\vec{\rho}_3, \vec{\rho}_2, \vec{v}t) \right\rangle \right) \right\rangle \quad \textbf{(15)}$$

and is given by Holmes as

$$C_\chi(\delta\vec{\rho}_3,\delta\vec{\rho}_2,\vec{v}\tau) = .132\,\pi^2 k^2 \int_o^1 C_n^2(t)dt \int_o^\infty du\, u^{-8/3} \sin^2\left[\frac{u^2 t(1-t)L}{2k}\right] J_o(u|\delta\vec{\rho}_3 t + \delta\vec{\rho}_2(1-t) - \vec{v}\tau|) \quad \textbf{(16)}$$

where t is the normalized pathlength, $t \equiv z/L$, from the target to the aperture, $\vec{r}_3$ is the transverse coordinate at the receiving aperture, $\vec{r}_2$ is at the target, and $\vec{v}$ is the transverse wind velocity.

Holmes has evaluated the aperture averaging integral of equations (11), (12) and (16) and found a numerically straightforward evaluation of equation (11) given by

$$s_{In}^2 = \sum_m b_m \left(2\exp\left[4C_c\left(d\vec{\rho}_3 = 0, d\vec{\rho}_2 = LP_m/kA, \vec{v}t = 0\right)\right] - 1\right) \quad \textbf{(17)}$$

where

$$b_m = \frac{2}{A^2 J_1^2(P_m)} \int_o^A x\, f_2(x)\, J_o\left(\frac{P_m}{A}x\right)dx \quad \textbf{(18)}$$

and A is an arbitrary integration point such that the integral beyond A in equation (18) becomes negligible, and P_m is the mth zero of $J_o(x)$. The log-amplitude covariance of equation (16) may then be evaluated using

$$C_\chi(\delta\vec{\rho}_3, \delta\vec{\rho}_2, \vec{v}\tau) = 0.132\,\pi^2 k^2 L\, C_n^2 \int_0^1 dt\, H(a, b) \quad \textbf{(19)}$$

where

$$H(a,b) = \frac{-3b^{5/3}\Gamma^2(1/3)}{20(\pi)^{1/2}\Gamma(11/6)}\cos\left(\frac{\pi}{6}\right) + \frac{3a^{5/3}}{5(2)^{1/6}}\Gamma\left(\frac{1}{6}\right) \times\left(\frac{\exp[i(\pi/12)]}{2i}\,{}_1F_1\left(\frac{-5}{6};1;-\frac{ib^2}{8a^2}\right) - \frac{\exp[-i(\pi/12)]}{2i}\,{}_1F_1\left(\frac{-5}{6};1;\frac{ib^2}{8a^2}\right)\right) \quad \textbf{(20)}$$

with ${}_1F_1$ being the confluent hypergeometric function and with

$$a^2 \equiv \left(t(1-t)L\right)/2k \quad \textbf{(21)}$$

and

$$b \equiv |d\vec{\rho}_3 t + d\vec{\rho}_2(1-t) - \vec{v}t| \quad \textbf{(22)}$$

Equations (16) through (20) are analytically complicated but may be numerically evaluated using the series expansions

$${}_1F_1(a;c;x) = \sum_{n=o}^{N} \frac{\Gamma(a+n)\,\Gamma(c)}{\Gamma(a)\,\Gamma(c+n)}\,\frac{x^n}{n!} \quad \textbf{(23)}$$

for small x or using

$${}_1F_1(a;c;x) = \Gamma(c)\left[\frac{e^{-i\pi a}x^{-a}}{\Gamma(c-a)}\sum_n \frac{\Gamma(a+n)\Gamma(1+a-c+n)}{\Gamma(a)\Gamma(1+a-c)}\frac{(-x)^n}{n!} + \frac{e^x x^{a-c}}{\Gamma(a)}\sum_n \frac{\Gamma(c-a+n)\Gamma(1-a-n)}{\Gamma(c-a)\Gamma(1-a)}\frac{x^n}{n!}\right] \quad \textbf{(24)}$$

for large x values. Some results are shown in **Figure 1**.

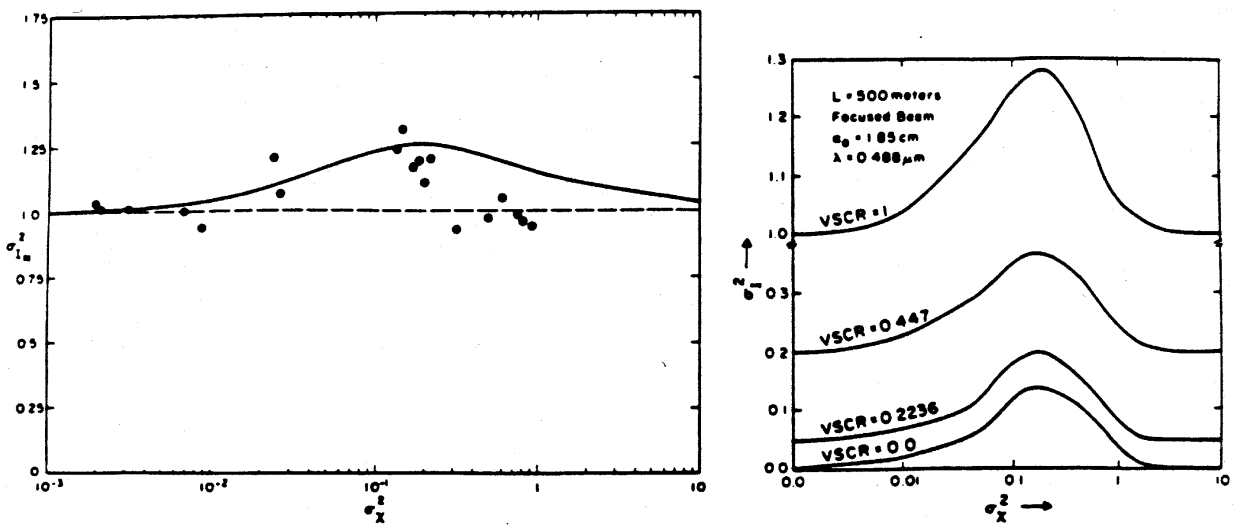

Figure 1. *A) Normalized variance of irradiance versus Rytov variance (point log-amplitude variance) for a resolved diffuse target illuminated by a coherent source. Solid line is the theoretical curve from Holmes[1-4] B) Same for multiple uncorrelated mode laser and coherent single mode laser. The "vacuum speckle contrast ratio" is the reciprocal of the number of uncorrelated laser modes, M_l.*

Many researchers use the inverse of the variance of the normalized intensity, equation (10), as the definition of SNR. As seen in **Figure 1**, the σ_I^2 determined from equations (11) through (24) is valid for strong round-trip turbulence and predicts considerable aperture averaging with nominal aperture sizes in good agreement with the data. At low turbulence conditions, the normalized intensity variance is 1.0 due to target speckle only. At high turbulence conditions the intensity variance is due entirely to scintillation, but the E-field again becomes a complex Gaussian random variable with Rayleigh distributed amplitude envelope and unit mean variance negative-exponential amplitude-squared envelope, the same as for pure speckle-targets. At intermediate turbulence levels, the scintillation is larger than one due to additional corruption of the speckle statistics by the turbulence.

2.3 A Simple Model of Scintillation Statistics from Resolved Targets for the K-distributions

Scintillation statistics for **resolved** diffuse targets have also been well established[1-4] with data and theory by Holmes and co-workers for low cross-wind, nearly static ladar and target conditions. (The results need to be modified for high slew rate, aircraft operation, or satellite operation corresponding to high Greenwood frequencies.) Path integrated turbulence strength is most often characterized by the Rytov variance or the **non**fluctuating **p**oint-source, **p**oint-receiver, **one-way** propagation "log-amplitude variance"

$$\sigma_{\chi p}^2(R) = 0.56\ k^{7/6} \int_o^R dz\ C_n^2(z)\,(z/R)^{5/6}\,(R-z)^{5/6} \qquad \textbf{(25)}$$

where $C_n^2(z)$ is the refractive index structure coefficient. (Note that the Rytov variance is **symmetric** with respect to the optical path. The same value is obtained whether we go from the ladar to the target or from the target to the ladar. As such, the value of the Rytov parameter for determining a ROC is questionable.) For constant C_n^2 equation (25) reduces to

$$\sigma_{\chi p}^2(R) = 0.124\, C_n^2 k^{7/6} R^{11/6} \quad (C_n^2 \text{ constant}) \qquad \textbf{(26)}$$

From weak turbulence theory, the normalized intensity variance is related to the Rytov parameter by

$$\sigma_{I_n}^2 = \exp(4\,\sigma_{\chi p}^2) - 1 \qquad \textbf{(27)}$$

Following references 1 to 4, we define the **aperture-averaged** normalized intensity variance or "scintillation parameter" as

$$\sigma_{In}^2 = \exp(\gamma 4\sigma_{\chi p}^2) - 1 + \frac{1}{M_l} \quad \textbf{(28)}$$

where σ_{In}^2 is the variance of the normalized intensity, which is reduced by aperture averaging via the factor γ, the aperture-averaging factor, and M_l is the number of independent laser modes. It is possible to make a simple curve fit to data and theory from Holmes et al. in **Figure 1**, and after some trial and error the aperture averaging factor

$$\gamma \approx \frac{0.6}{1 + 100\,\sigma_{\chi p}^4} \quad \textbf{(29)}$$

appears to give a good simple fit to the data and theory.

The PDF's of the roundtrip scintillation for **coherent detection** have been shown experimentally and theoretically[4] to be well described by the **monochromatic K-distribution** (**Figure 2**) given by

$$p_I(I) = 2\left(\frac{M_t}{<I>}\right)^{(M_t+1)/2} \frac{I^{(M_t-1)/2}}{\Gamma(M_t)} K_{M_t-1}\left(2\left(\frac{M_t I}{<I>}\right)^{1/2}\right) \quad \textbf{(30)}$$

or normalized

$$p_{I_n}(I_n) = \left(2\,M_t^{(M_t+1)/2} I_n^{(M_t-1)/2}/\Gamma(M_t)\right) K_{M_t-1}\left(2\left(M_t I_n\right)^{1/2}\right) \quad \textbf{(31)}$$

where M_t is the turbulence strength parameter, and $K_{Mt-1}(I)$ is a modified Bessel function of order M_t-1 for coherent detection of a single mode laser. M_t must be determined from

$$\sigma_{I_n}^2 \equiv \frac{<I^2> - <I>^2}{<I>^2} = 1 + \frac{2}{M_t} \quad \textbf{(32)}$$

for use in equations (30) or (31) from equations (28) and (29) with $M_l = 1$.

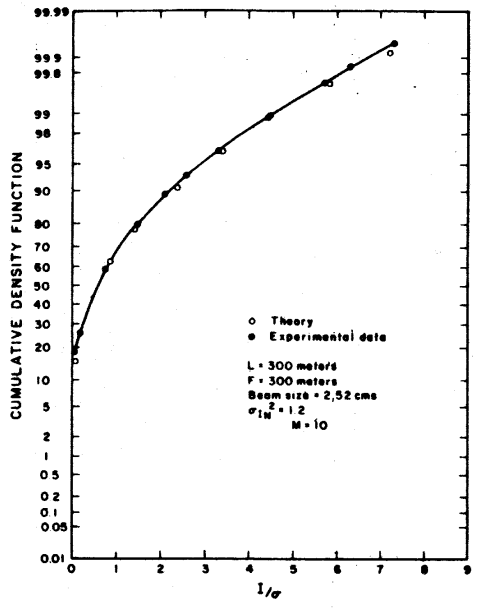

Fig. 1. Comparison of experimental cumulative PDF with theory for a monochromatic speckle pattern, 300-m path length.

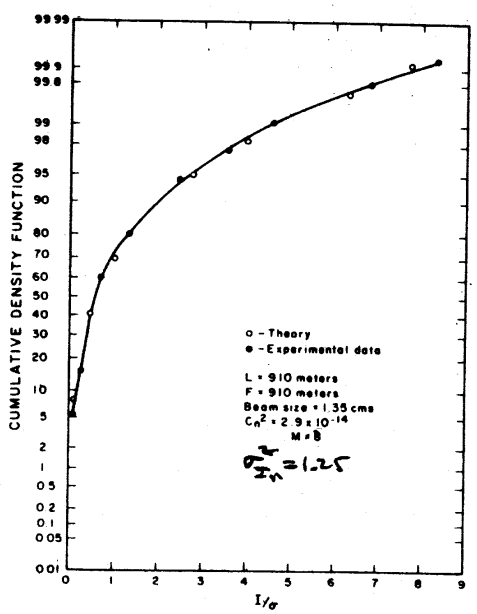

Fig. 2. Comparison of experimental cumulative PDF with theory for a monochromatic speckle pattern, 910-m path length.

Figure 2*. Monochromatic K-distribution data fit.*

For **direct detection** using a **multimode laser**, the scintillation PDF is given by the **polychromatic K-distribution** of

$$p_I(I) = \frac{(M_l\, M_t)^{(M_l+M_t)/2}}{\Gamma(M_l)\Gamma(M_t)} \frac{2I^{(M_l+M_t)/2-1}}{\langle I\rangle^{(M_l+M_t)/2}} K_{|M_l-M_t|}\left(2\left(\frac{M_l M_t I}{\langle I\rangle}\right)^{1/2}\right) \quad \textbf{(33)}$$

or normalized

$$p_{I_n}(I_n) = \frac{(M_l\, M_t)^{(M_l+M_t)/2}}{\Gamma(M_l)\Gamma(M_t)} 2\, I_n^{(M_l+M_t)/2-1} K_{|M_t-M_l|}\left(2\left(M_l\, M_t\, I_n\right)^{1/2}\right) \quad \textbf{(34)}$$

where M_l is the number of uncorrelated laser modes, and the normalized intensity variance is used to determine M_t

$$\sigma^2_{I_n} = \left(1+\frac{1}{M_l}\right)\left(1+\frac{1}{M_t}\right)-1 \quad \textbf{(35)}$$

and M_l must be determined by other measurements. **Figure 3** shows good experimental and theortetical agreement for resolved targets.

2.4 Scintillation from Unresolved Targets (An Extrapolation)

Scintillation statistics for **unresolved** glint targets have been measured and numerically analyzed by Churnside et al[5-6] as shown in **Figure 4**. A simple curve fit to these data relating the Rytov variance to the unresolved-target round-trip scintillation parameter in **Figure 4** has been found to be

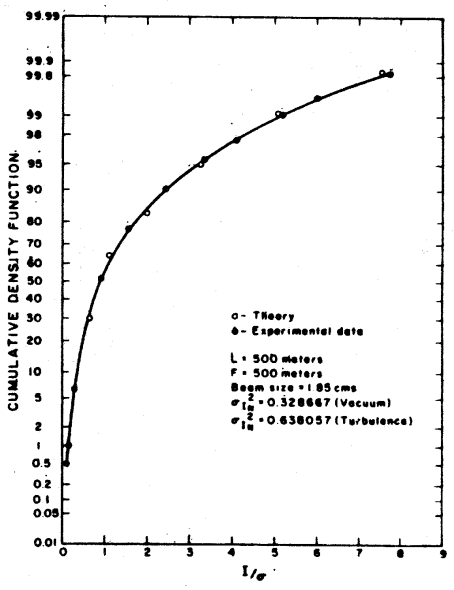

Fig. 3. Comparison of experimental cumulative PDF with theory for a polychromatic speckle pattern, $\sigma_{IN}^2 = 0.638$.

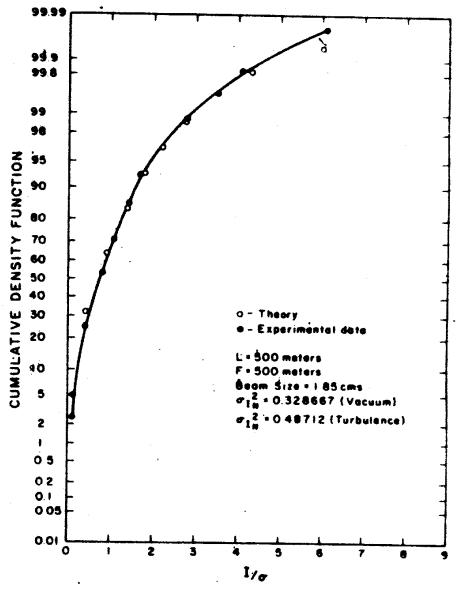

Fig. 4. Comparison of experimental cumulative PDF with theory for a polychromatic speckle pattern, $\sigma_{IN}^2 = 0.487$.

Figure 3. *Polychromatic K-distribution data fit.*

$$\sigma^2_{In} = \exp(\gamma 4\,\sigma^2_{\chi p})-1+\frac{1}{M_l} \qquad \gamma \equiv \frac{12}{1+250\,\sigma^4_{\chi p}} \quad \textbf{(36)}$$

here $M_l = 1$ for coherent single mode lasers. (See **Figure 5**.) Since these data were collected for a 1 mm pupil, aperture averaging will reduce the scintillation, and for calculations we follow Churnside[7]

$$\sigma^2_{I_n avg} = A_{Ch}\,\sigma^2_{I_n} \quad \textbf{(37)}$$

where

$$A_{Ch}(R) = \frac{\sigma_{I_n}^2(R)+1}{2\sigma_{I_n}^2(R)}\left(1+\left(\frac{D}{3\rho_o(R)}\right)^2\right)^{-1} + \frac{\sigma_{I_n}^2(R)-1}{2\sigma_{I_n}^2(R)}\left(1+0.6\left(\frac{kD1.5\rho_o(R)}{2R}\right)^{7/3}\right)^{-1} \quad \textbf{(38)}$$

for the strong turbulence cases of both

$$\rho_o < (L/k)^{1/2} (Fresnel\ zone)\ \ with\ \ \rho_o \le l_o\ \ or\ \ \rho_o > l_o \quad \textbf{(39)}$$

2.5 Implications for the Receiver-Operating-Characteristic

We propose that the **unresolved** target scintillation index should then be used in the K-distributions (equations (30-31) and (34-35)) of Section 2.3, which are derived for **resolved** targets, to compute probabilities of detection vs false alarm rates in a receiver-operating-characteristic analysis. For example, for heterodyne detection, the ROC should be given by[8]

$$P_D = \int_o^\infty p_{pK}(I_n)\, P_F^{(1+CNR_s I_n)^{-1}}\, dI_n \quad \textbf{(40)}$$

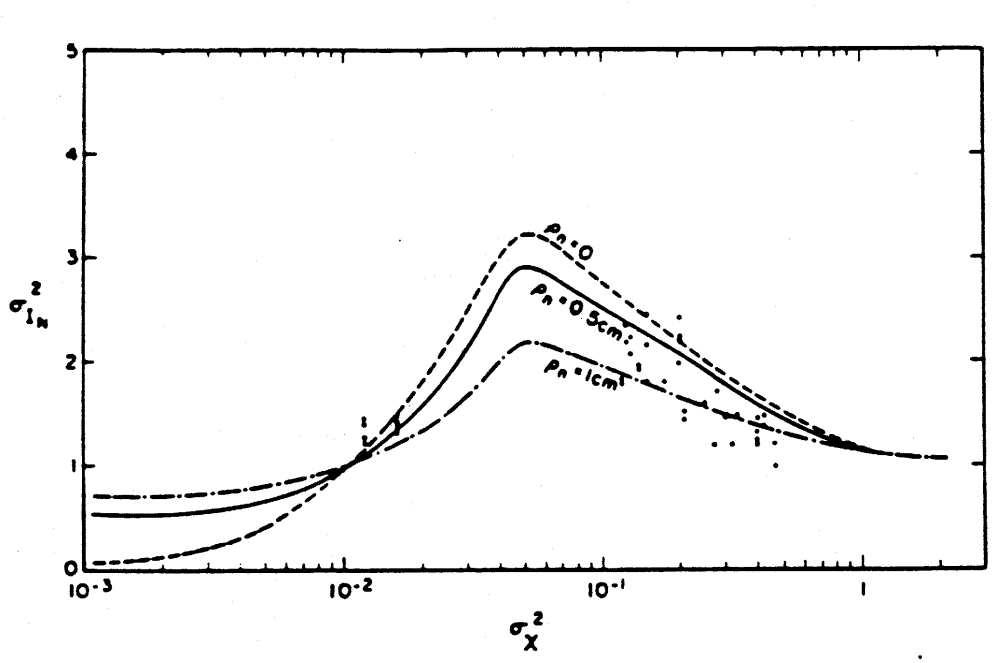

Figure 4. *Normalized variance of irradiance versus Rytov variance for a resolved large diffuse target with a single small glint in front illuminated by a coherent laser. Experimental points are indicated by dots, and the numerical analyses from Churnside[6] are indicated by lines for the three off-axis distances as indicated.*

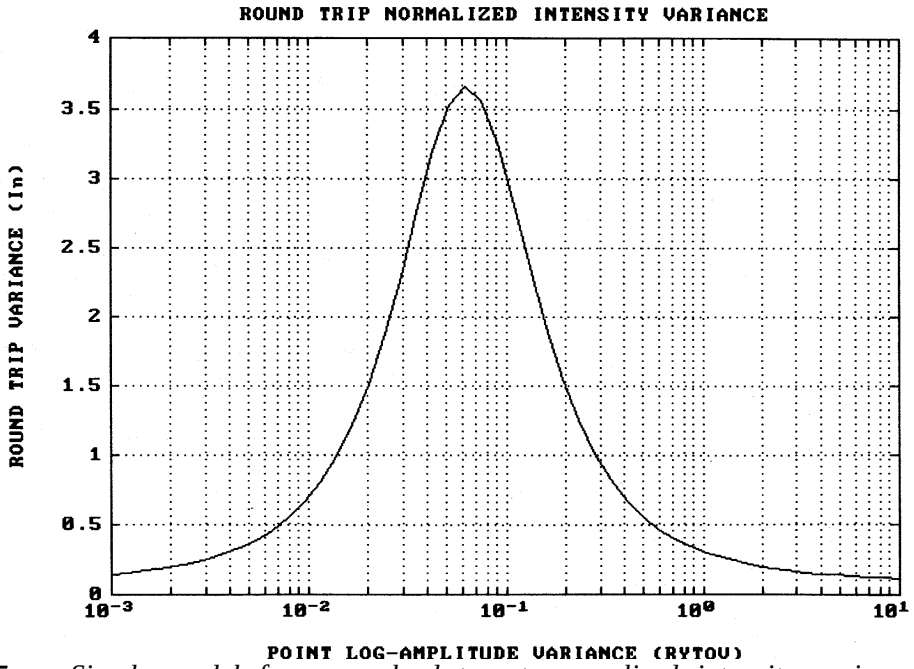

Figure 5. *Simple model for unresolved target normalized intensity variance vs Rytov parameter.*

where p_{pK} is the polychromatic K-distribution with M_l = infinity, since a diffuse target (σ_{ln} = 1) has been included already in equation (36) and, therefore, equation (40). The PDF would then in actuality be an atmospheric turbulence only effect.

3.0 MONTE CARLO SIMULATION CODE DESCRIPTION

The Monte Carlo code[9,10] simulating the physical processes (analytically) described above is illustrated in **Figure 6**. The laser source propagates from the ladar aperture on the left side of the figure represented by an E-field at the center of a 2D grid of E-field elements. The mode is defined to be a Gaussian plane wave with a beam-waist radius dimension defined by the ladar being modeled. The beam waist radius is smaller than the transmitting telescope aperture radius depending on the desired field-of-view ladar. The laser mode E-field is then propagated a distance δz through the first phase screen using a split-step Fourier algorithm

$$E(x,y,z+\delta) = \Im_2^{-1}\left(\exp(-iA\delta)\Im_2\left(\exp(i\theta(x,y))E(x,y,z)\right)\right) \quad \textbf{(41)}$$

where

$$A = \kappa^2 / 2k \quad \textbf{(42)}$$

and $\boldsymbol{\kappa}$ is the wavenumber vector (κ_x, κ_y) with magnitude κ. The phase increment $\theta(x,y)$ due to propagation through a phase screen j is given by

$$\theta_j(x,y) = k\int_{z_j-\delta/2}^{z_j+\delta/2} n(x,y,u)du \quad \textbf{(43)}$$

where at each step θ is generated by the inverse Fourier transform of a filtered white Gaussian pseudorandom field which constrains the power spectrum of the phase fluctuations to the desired spectrum such as the modified Kolmogorov spectrum

$$\Phi(\kappa) = 0.033\, C_n^2\left(\kappa^2 + 1/L_o^2\right)^{-11/6}\exp\left(-\kappa^2/(l_o/5.92)^2\right) \quad \textbf{(44)}$$

where C_n^2 is the refractive index constant L_o is the outer scale of turbulence and l_o is the inner scale of turbulence. L_o is typically the lesser of 10 m or the height of the laser beam above the ground or the size of an open window. The inner scale of turbulence is typically 1 to 10 mm.

The propagation steps are repeated, typically with 20 to 40 screens, until the range to target is reached. The E-field matrix at the target is then clipped to represent the target's cross-sectional area, varying in this study from 10 cm x 10 cm to 51 cm x 51 cm in size. Random phasors within the target area represent a diffuse target surface. The back-scattered speckle-pattern then passes in reverse order through the random phase screens. If there is little transverse wind, say in sea-skimmer detection on a calm day, the same random phase screens are used. If there is a strong transverse wind, say in side-looking ladar on aircraft, new (independent) random phase screens are generated for the return path. The final E-field matrix is then stored. The scintillation statistics, resulting from many phase-screen realizations, at one E-field matrix point corresponds to a point aperture (about 1 mm in diameter) produced scintillation. By averaging over many 1 mm apertures, we can simulate the effects of aperture averaging for a given target size. Typical aperture sizes are 10 cm to 25 cm in diameter. There are obviously many combinations of target, aperture, range, l_o, and C_n^2 values. Each round-trip turbulence realization requires about 100 Gflops and at least 20 realizations are required for good statistics, thus, the Monte Carlo simulation study is quite computer intensive.

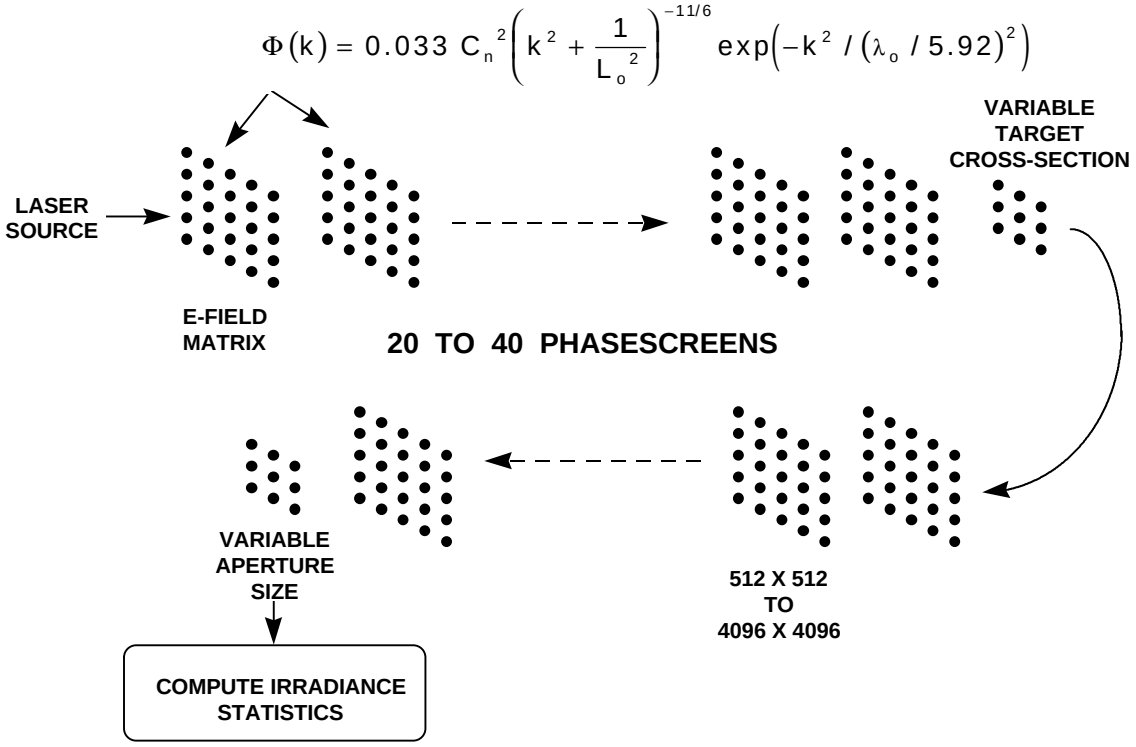

Figure 6. *Round-trip turbulence Monte Carlo Analysis schematic.*

4.0 MONTE CARLO SIMULATION RESULTS TO DATE

The initial series of computer runs pertained to Navy sea-skimmer detection scenarios using an eyesafe 1.5 μm laser and constant C_n^2 values with the same phase-screens inward and outward, inner scales

of 1 to 10 mm, a 20 km maximum range, 10 cm to 25 cm diameter apertures, and 10x10 cm^2 to 51x51 cm^2 target cross-sections.

4.1 Validation of the K-Distribution for Normalized-Intensity Fluctuation (Scintillation)

The monochromatic K-distribution pdf (K-pdf) of equations (30-31) is compared to the lognormal pdf (logN) and the exponentially modulated lognormal pdf (logNexp) which are often used to model scintillation. The goodness of fit to the Monte Carlo simulation results is determined by computing the third and fourth moments of the normalized intensity, known as skewness and kurtosis:

$$skewness = \langle (I - \langle I \rangle)^3 \rangle \quad \textbf{(45)}$$

$$kurtosis = \langle (I - \langle I \rangle^4 \rangle - 3 \langle (I - \langle I \rangle)^2 \rangle^2 \quad \textbf{(46)}$$

$$variance = \sigma_I^2 = \left\langle \left(I - \langle I \rangle \right)^2 \right\rangle \quad \textbf{(47)}$$

For a 20.5 km target range with nearly constant $C_n^2 = 1 \times 10^{-18}$, we obtain the following fits vs target size for the two extreme values of l_o:

Inner Scale = l_o = 1 mm

Target Sizes:	**51x51 cm^2**	**40x40 cm^2**	**30x30 cm^2**	**20x20 cm^2**	**10x10 cm^2**
Variance	1.230	1.597	2.040	2.283	32.693
Skewness (simul.)	3.47	7.134	10.35	14.05	49.63
Skewness (K-pdf)	3.65	11.14	18.33	22.45	52.04
Skewness (logN/exp)	3.74	11.81	20.79	26.5	77.54
Skewness (logN)	6.25	2.77	0.94	0.15	0.004
Kurtosis (simul.)	15.50	64.36	82.83	132.76	1215
Kurtosis (K-pdf)	17.29	64.69	165.93	249.81	1042
Kurtosis (logN/exp)	18.79	83.72	268.08	453.40	3999
Kurtosis (logN)	81.89	35.85	11.96	1.36	0.02

Inner Scale = l_o = 10 mm

Target Sizes:	**51x51 cm^2**	**40x40 cm^2**	**30x30 cm^2**	**20x20 cm^2**	**10x10 cm^2**
Variance	1.23	**	2.01	**	2.70
Skewness (simul.)	3.47	**	8.91	**	23.70
Skewness (K-pdf)	3.65	**	17.91	**	29.92
Skewness (logN/exp)	3.73	**	20.20	**	37.92
Skewness (logN)	6.25	**	0.68	**	0.004
Kurtosis (simul.)	15.49	**	57.60	**	400
Kurtosis (K-pdf)	17.26	**	159.91	**	420
Kurtosis (logN/exp)	18.75	**	252.75	**	953
Kurtosis (logN)	81.76	**	7.43	**	0.01

Obviously the K-pdf fit is better than the exponentially-modulated-lognormal pdf and is much better than the lognormal pdf. We note that for the small inner scale (1 mm) the variance of the normalized intensity becomes quite large for the smaller targets due to smaller atmospheric-speckle averaging by the smaller target cross-sections. This variance pertains to the 1 mm sample point apertures and will be reduced by receiver aperture averaging which is currently under investigation.

4.2 Stronger Turbulence Cases

In stronger path integrated turbulence situations with larger C_n^2 values than treated above at 20.5 km range, the polychromatic K-distribution (equations (33-34)) has been found to give a better fit to the Monte Carlo results. One M parameter (M_t) represents the effects the turbulent atmosphere on a coherent beam alone, and the second M parameter (M_l) is redefined to be the ratio of the correlation length of the wave on the target after propagation through turbulence ($\rho_o(R)$) divided by the target size. The normalized intensity moments[4] out to 6th order give good matches to the simulation results. For the conditions treated in Section 4.1 ($C_n^2 = 1x10^{-18}$ at 20.5 km range) and choosing the inner scale (l_o) to be 1 mm, we re-examine the 20 x 20 cm^2 and 30 x 30 cm^2 target size cases which showed the worst fit to the model pdf's. The normalized intensity (equation (10)) moments are found to be:

20 cm x 20 cm Target

	$\langle I_n^4 \rangle$	$\langle I_n^5 \rangle$	$\langle I_n^6 \rangle$
simulation	22.84	105.12	549.03
polyK-pdf	23.12	110.57	622.89

30 cm x 30 cm Target

	$\langle I_n^4 \rangle$	$\langle I_n^5 \rangle$	$\langle I_n^6 \rangle$
simulation	150.80	1727.64	24387
polyK-pdf	159.33	2097.18	37478

The fit to the Monte Carlo runs is seen to be better than that of the monochromatic K-distribution used in Section 4.1. Higher C_n^2 values are currently being examined, but these runs require larger E-field matrices of about 4096 x 4096 dimension, therefore, requiring the use of super-computers. These results will be reported at a later date.

4.3 Aperture Averaging Effects

The received E-field 1 mm point-aperture intensities for any individual Monte Carlo run may be collected in groups of 100x100, 200x200, 300x300, etc. to simulate larger aperture telescope receivers of 10, 20, and 30 cm width, respectively. Smoothed intensity fluctuations (i.e., reduced scintillation index, σ_{In}^2) are found using a larger aperture telescope, and the aperture averaging reduction of the scintillation index has been found to be in good agreement with theory[7] in our preliminary runs. For shorter and more tractable propagation paths of 1 to 2 km, we are operating in the near field. The effects of (outward) turbulence produced speckle averaging by the target's finite cross-range extent have been observed as shown in **Figure 7**. For a 1070 m path and $C_n^2 = 2 \times 10^{-14}$ at 1.55 μm, as the target cross-range dimension

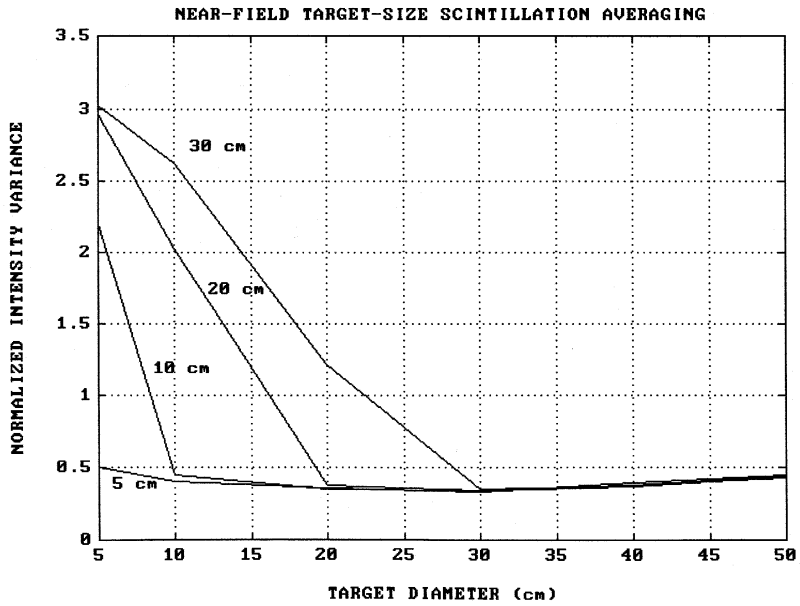

Figure 7*. Scintillation averaging by finite target cross-range size. The scintillation index is computed versus target cross-range dimension for four different receiving aperture diameters for a 1070 m path and* $C_n^2 = 2 \times 10^{-14}$ *at 1.55* mm

becomes larger, it subtends more turbulence produced speckle maxima, thus decreasing round-trip scintillation. It is interesting to note that when the target cross-range dimentsion becomes equal to the the receiving aperture diameter, the scintillation is greatly reduced. The effects of finite target-size smoothing as the target moves into the far-field, at around 20 km in range, are also currently being investigated.

5.0 SUMMARY AND STATUS OF CURRENT SIMULATIONS

The simulation of stronger C_n^2 paths is continuing using larger E-field and phase perturbation matrices. The use of a Cray super-computer has recently become available courtesy of the Space and Strategic Defense Command in Huntsville, Ala. to do these simulations. The refinement of the polychromatic K-distribution to model target speckle-averaging (M_l parameter) and return trip turbulence (M_t parameter) is continuing, and it appears to be an excellent pdf choice for strong path integrated turbulence cases so far. For weaker path-integrated turbulence cases, the monochromatic K-distribution (single parameter) gives an excellent fit to the simulations. In addition, stronger transverse wind scenarios, as for side pointing aircraft mounted ladars, will be analyzed by generating new random phase-screens for the return path (close to the A/C) instead of saving the outgoing phase-screens for back-propagation. These new pdf's may then be incorporated into a correct ladar receiver-operating-characteristic.

6.0 ACKNOWLEDGEMENTS

This work was funded jointly by the Advanced Sensors Technology Program (ASTP) of the Ballistic Missile Defense Organization, Dr. Walter Dyer technical manager, and the AWACS/EAGLE (ground test phase) ladar program funded by Texas Instruments, Dennis Womack technical manager. The E-field propagation code was made available by Prof. Stanley Flatte at the University of California, Santa Cruz.

7.0 REFERENCES

1. M. Lee, F. Holmes, R. Kerr, "Statistics of speckle propagation through the turbulent atmosphere," J. Opt. Soc. Am. 66, Nov. 1976.

2. F. Holmes, M. Lee, R. Kerr, "Effect of the log-amplitude covariance function on the statistics of speckle propagation through the turbulent atmosphere," J. Opt. Soc. Am. 70, April 1980.

3. R. Gudimetla, F. Holmes, R. Elliott, "Two-point joint-density function of the intensity for a laser-generated speckle field after propagation through the turbulent atmosphere," J. Opt. Soc. Am. A 7, June 1990.

4. R. Gudimetla, F. Holmes, "Probability density function of the intensity for a laser-generated speckle field after propagation through the turbulent atmosphere," J. Opt. Soc. Am., Vol. 72, Sept. 1982.

5. C. McIntyre, Kerr, Lee, Churnside, "Enhanced variance of irradiance from target glint," Appl. Opt. 18, 1 Oct. 1979.

6. C. McIntyre, Lee, Churnside, "Statistics of irradiance scattered from a diffuse target containing multiple glints," J. Opt. Soc. Am. 70, Sept. 1980.

7. J. Churnside, "Aperture averaging of optical scintillations in the turbulent atmosphere," Appl. Opt. 30, 1991.

8. J. Shapiro, B. Capron, R. Harney, "Imaging and target detection with a heterodyne-reception optical radar," Appl. Opt., Vol. 20 No. 19, 1 Oct. 1981.

9. J. Martin, S. Flatte, "Intensity images and statistics from numerical simulation of wave propagation in 3-D random media," Appl. Opt. 27, No. 11, 1 June 1988.

10. J. Martin, S. Flatte, "Simulation of point-source scintillation through three-dimensional random media," J. Opt. Soc. Am. A, Vol. 7, May 1990.

11. S. Flatte et al., "Irradiance variance of optical waves through atmospheric turbulence by numerical simulation and comparison with experiment," J. Opt. Soc. Am., Vol. 10, Nov. 1993.

12. S. Flatte et al., "Probability-density functions of irradiance for waves in atmospheric turbulence calculated by numerical simulation," J. Opt. soc. Am. A, Vol. 11, 1994.